

Dynamical universality classes of simple growth and lattice gas models

Jeffrey Kelling (2,3), Géza Ódor (1) and Sibylle Gemming (3,4)

(1) *Institute of Technical Physics and Materials Science,
Centre for Energy Research of the Hungarian Academy of Sciences
P.O.Box 49, H-1525 Budapest, Hungary*

(2) *Department of Information Services and Computing,
Helmholtz-Zentrum Dresden-Rossendorf
P.O.Box 51 01 19, 01314 Dresden, Germany*

(3) *Institute of Ion Beam Physics and Materials Research
Helmholtz-Zentrum Dresden-Rossendorf
P.O.Box 51 01 19, 01314 Dresden, Germany*

(4) *Institute of Physics, TU Chemnitz
09107 Chemnitz, Germany*

Large scale, dynamical simulations have been performed for the two dimensional octahedron model, describing Kardar–Parisi–Zhang (KPZ) for nonlinear, or Edwards–Wilkinson (EW) for linear surface growth. The autocorrelation functions of the heights and the dimer lattice gas variables are determined with high precision. Parallel random-sequential (RS) and two-sub-lattice stochastic dynamics (SCA) have been compared. The latter causes a constant correlation in the long time limit, but after subtracting it one can find the same height functions as in case of RS. On the other hand the ordered update alters the dynamics of the lattice gas variables, by increasing (decreasing) the memory effects for nonlinear (linear) models with respect to RS. Additionally, we support the KPZ ansatz and the Kallabis-Krug conjecture $\lambda_C = D$ in $2 + 1$ dimensions and provide a precise growth exponent value $\beta = 0.2414(2)$. We show the emergence of finite size corrections, which occur much earlier than the height saturation.

PACS numbers: 05.70.Ln, 05.70.Np, 82.20.Wt

I. INTRODUCTION

Nonequilibrium systems are known to exhibit dynamical scaling, when the correlation length diverges as $\xi \propto t^{1/z}$, characterized by the exponent z . Simplest models are driven lattice gases (DLG) [1], which in certain cases can be mapped onto surface growth [2, 3]. Therefore, understanding DLGs, which is far from being trivial due to the broken time reversal symmetry [4], and is possible mostly by numerical simulations only, sheds some light on the corresponding interface phenomena [5]. The simplest example is the asymmetric simple exclusion process (ASEP) of particles [6], in which particles and holes can be mapped onto binary surface slopes [7, 8] and the corresponding continuous model can be described by the Kardar–Parisi–Zhang (KPZ) equation [9]

$$\partial_t h(\mathbf{x}, t) = \sigma \nabla^2 h(\mathbf{x}, t) + \lambda (\nabla h(\mathbf{x}, t))^2 + \eta(\mathbf{x}, t), \quad (1)$$

where the scalar field $h(\mathbf{x}, t)$ is the height, progressing in the D dimensional space relative to its mean position, that moves linearly with time t . This equation was inspired in part by the stochastic Burgers equation [10] and can describe the dynamics of simple growth processes in the thermodynamic limit [11], randomly stirred fluids [12], directed polymers in random media [13], dissipative transport [14, 15], and the magnetic flux lines in superconductors [16]. In case of surface growth σ represents a surface tension, competing with the nonlinear up–down anisotropy of strength λ and a zero mean valued Gaussian white noise. This field exhibits the variance $\langle \eta(\mathbf{x}, t) \eta(\mathbf{x}', t') \rangle = 2\Gamma \delta^D(\mathbf{x} - \mathbf{x}') (t - t')$, with an

amplitude, related to the temperature in the equilibrium system, averaged over the distribution. The $\lambda = 0$, linear equation describes the Edwards–Wilkinson (EW) [17] surface growth, an exactly solvable equilibrium system.

Several discretized versions have been studied [2, 7, 18]. In these models the morphology of a surface of linear size L is usually described by the squared interface width

$$W^2(L, t) = \frac{1}{L^2} \sum_{i,j}^L h_{i,j}^2(t) - \left(\frac{1}{L} \sum_{i,j}^L h_{i,j}(t) \right)^2. \quad (2)$$

In the absence of any characteristic length simple growth processes are expected to be scale-invariant

$$W(L, t) \propto L^\alpha f(t/L^z), \quad (3)$$

with the universal scaling function $f(u)$:

$$f(u) \propto \begin{cases} u^\beta & \text{if } u \ll 1 \\ \text{const.} & \text{if } u \gg 1 \end{cases} \quad (4)$$

Here α is the roughness exponent in the stationary regime, when ξ has exceeded L and β is the growth exponent, describing the intermediate time behavior. The dynamical exponent z can be expressed as the ratio of the growth exponents:

$$z = \alpha/\beta \quad (5)$$

In two as well as in higher dimensions not much is known analytically about the scaling behavior of the KPZ

equation (1). The Galilean symmetry [12] implies the scaling relation:

$$2 = \alpha + z = \alpha(1 + 1/\beta) \quad (6)$$

This equation relates the roughness to the dynamical and growth exponents, allowing one to check numerically obtained estimates for consistency.

Apart from the exponents, the shapes of the rescaled width and height distributions of the interfaces $\Psi_L(\varphi_L)$ were shown to be universal in KPZ models [19, 20]. In fact many people define the universality classes by these quantities, which can be obtained exactly in one dimension [21, 22]. Here, φ_L denotes the interface observable in question, W^2 or h , in a system of linear size L . The non-rescaled probability distributions are denoted by $P_L(\varphi_L)$ and their moments are defined via the distribution averages as:

$$\Phi_L^n[\varphi_L] = \int_0^\infty (\varphi_L - \langle \varphi_L \rangle)^n P_L(\varphi_L) d\varphi_L \quad , \quad (7)$$

Two standard measures of the shape, the skewness

$$S_L[\varphi_L] = \langle \Phi_L^3[\varphi_L] \rangle / \langle \Phi_L^2[\varphi_L] \rangle^{3/2} \quad (8)$$

and the kurtosis

$$Q_L[\varphi_L] = \langle \Phi_L^4[\varphi_L] \rangle / \langle \Phi_L^2[\varphi_L] \rangle^2 - 3 \quad , \quad (9)$$

are calculated usually, often in the steady state. The universal, rescaled forms are:

$$\Psi_L[W^2(L)] = \langle W^2(L) \rangle P_L(W^2(L) / \langle W^2(L) \rangle) \quad (10)$$

for the width and

$$\Psi_L[h_L(r)] = L^\alpha P_L(h_L(r) / L^\alpha) \quad (11)$$

for the surface height. Note, that $\langle h_L \rangle \equiv \Phi_L^0[h_L] \equiv 0$ in the co-moving frame of the surface.

While many systems are described by a single dynamical length scale, aging ones are best characterized by two-time quantities, such as the dynamical correlation and response functions [23]. In the aging regime: $s \gg \tau_m$ and $t - s \gg \tau_m$, where τ_m is a microscopic time scale and s is the start time, when the snapshot is taken, one expects the following law for the autocorrelation function

$$C(t, s) = \langle \phi(t, \mathbf{r}) \phi(s, \mathbf{r}) \rangle - \langle \phi(t, \mathbf{r}) \rangle \langle \phi(s, \mathbf{r}) \rangle \quad (12)$$

$$\propto s^{-b} (t/s)^{-\lambda_C/z} \quad , \quad (13)$$

here $\langle \rangle$ denotes averaging over the sites and independent samples, λ_C is the autocorrelation and b is the aging exponent. The function ϕ denotes the measured quantity, which can be the particle density of the lattice gas or the

surface height $h(t, \mathbf{r})$. In the latter case, for $t = s$ one finds:

$$\begin{aligned} C_h(t, s) &= \langle h(t, \mathbf{r}) h(t, \mathbf{r}) \rangle - \langle h(t, \mathbf{r}) \rangle \langle h(t, \mathbf{r}) \rangle \\ &= \langle h^2(t, \mathbf{r}) \rangle - \langle h(t, \mathbf{r}) \rangle \langle h(t, \mathbf{r}) \rangle \\ &= W^2(L \rightarrow \infty, t) \propto s^{-b_h} \cdot f_C(1) \quad . \end{aligned}$$

This implies the relation

$$b_h = -2\beta \quad , \quad (14)$$

which must be satisfied in the $L \rightarrow \infty$ and $s \rightarrow \infty$ limit. We have also calculated the auto-correlation of the slope (density) variables

$$\begin{aligned} C_s(t, s) &= \langle (n(t; \vec{r}) - \langle \bar{n}(t; \vec{r}) \rangle) (n(s; \vec{r}) - \langle \bar{n}(s; \vec{r}) \rangle) \rangle \\ &= \langle n(t; \vec{r}) n(s; \vec{r}) \rangle - \langle \bar{n}(t; \vec{r}) \rangle \langle \bar{n}(s; \vec{r}) \rangle \\ &= s^{-b_s} f'_C \left(\frac{t}{s} \right) \quad , \end{aligned} \quad (15)$$

where $n(t; \vec{r})$ is the occupancy of the sites. However, $C_s(t, s)$ decays much faster than the height auto-correlator and obtaining reasonable signal/noise ratio requires much higher statistics.

A dynamic, perturbative renormalization group (RG) analysis of KPZ [24, 25] suggested that the short and the long time scaling behavior of the correlation function are identical and deduced a scaling relation for the short-time exponent

$$\theta = (D + 4)/z - 2 \quad . \quad (16)$$

Since $\theta = \lambda_C/z + 2\beta$, relation (16) holds in the exactly solvable $1 + 1$ dimensional case. In $D \geq 2$ dimensions perturbative RG can't access the strong coupling KPZ fixed point [26], thus the validity of this law should be tested by precise exponent estimates.

A conjecture based on a purely geometric argument, advanced by [27], which can also be deduced from the scaling relation (16) claims $D = \lambda_C$ in any dimensions. While it is certainly true in one dimension, we will also provide numerical evidence for the validity in $D = 2$.

In aging systems a similar scaling form is expected for the autoresponse function of the field ϕ :

$$R(t, s) = \left. \frac{\delta \langle \phi(t) \rangle}{\delta j(s)} \right|_{j=0} = s^{-1-a} f_R \left(\frac{t}{s} \right) \quad (17)$$

where j is the external conjugate to ϕ and a denotes the so-called aging exponent. The universal scaling function exhibits the asymptotic behavior $f_R(t/s) \sim (t/s)^{-\lambda_R/z}$ with the autoresponse exponent λ_R . In equilibrium $\lambda_C = \lambda_R$ and $a = b$ due to the fluctuation-dissipation (FD) symmetry [28]. In nonequilibrium systems these exponents can be completely independent. Therefore, we shall determine them one-by-one and investigate if some extended FD relation may occur among them. This will be done using our very recent aging response exponents [29], which were determined to test the validity of the logarithmic extension of local scale-invariance (LSI) [28] proposed by [30].

II. MODELS AND SIMULATION ALGORITHMS

Discrete models set up for KPZ have been studied a lot in the past decades [2, 7, 18]. A mapping between KPZ surface growth in two dimensions and driven lattice gases has been advanced in [31, 32] an extension of the "rooftop" model of [7, 8]. We call it octahedron model, which is characterized by binary slope variables $\sigma_{x/y}$ at the edges connecting the vertexes of octahedra [33]. The $\sigma_{x/y}$ take the values 0 or 1 to encode down or up slopes, respectively. Thus deposition or removal of octahedra corresponds to a stochastic cellular automaton with the simple Kawasaki update rules

$$\begin{pmatrix} 0 & 1 \\ 0 & 1 \end{pmatrix} \xrightarrow[p]{q} \begin{pmatrix} 1 & 0 \\ 1 & 0 \end{pmatrix} \quad , \quad (18)$$

where p and q denote the acceptance probabilities. Projecting the edges onto a plane yields a square lattice of slopes, which can then be considered as occupancy variables. This maps the octahedron model onto self-reconstructing dimers following an oriented migration along the bisection of the x and y directions of the surface (see Fig. in [32]). In this picture the surface heights must be defined relative to a reference point $h_{1,1} = 0$ and can be reconstructed from the slope variables as

$$h_{i,j} = \sum_{l=1}^i [2\sigma_x(l,1) - 1] + \sum_{k=1}^j [2\sigma_y(i,k) - 1] \quad . \quad (19)$$

Discrete surface and DLG models usually apply random sequential dynamics. On the other hand in certain cases synchronous, so called stochastic cellular automaton (SCA)-like site updating can prove to be useful, especially for simulations on parallel computers. This study is based on massively parallel simulations on graphics cards (GPUs). Synchronous updating in case of one-dimensional ASEP models has already been investigated [34–36]. One-point quantities in the bulk, like particle current or surface growth have been shown to exhibit the same behavior as in case of random-sequential (RS). However, n -point correlation functions may be different.

Here we extend the parallel two-sublattice scheme developed for ASEP [35] to the two dimensional dimer model as shown on Fig. 1, and compare the dynamical scaling results with those of the RS dynamics. Since blocks of sites to be updated can be visited in a sequential order within a sub-lattice step, the SCA dynamics can be implemented very efficiently [37], matching perfectly parallel processors of GPU architectures [38].

Performing RS simulations on GPUs is less straightforward, because unwanted correlations may be introduced [39]. In order to eliminate these and to achieve results as close to really sequential simulations as possible, we use a new domain decomposition (DD) scheme, which we call DTrDB. Details of the new implementation are documented elsewhere [40].

In order to estimate the asymptotic values of different exponents for $t \rightarrow \infty$, local slope analyses of the scal-

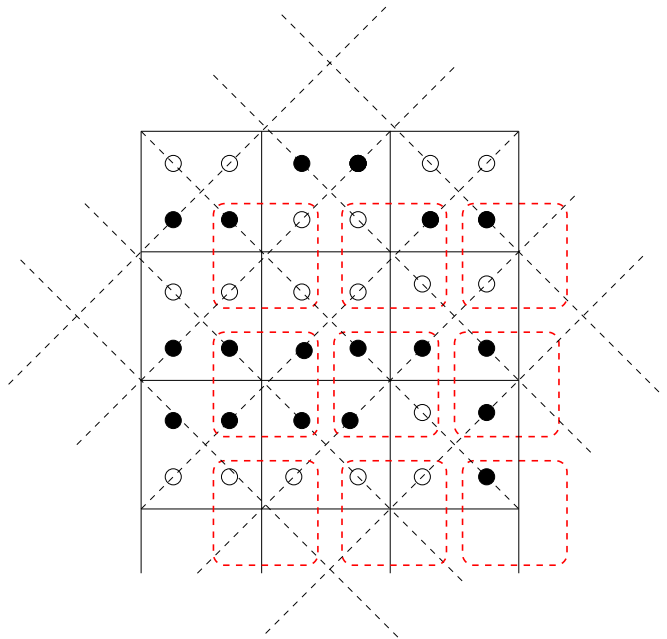


FIG. 1: Schematics of the two sub-lattice SCA updates of the dimer lattice gas model. Circles: empty sites (down slopes), bullets: filled sites (up slopes). Solid, black lines denote areas, where the rule (18) is applied at t odd, while dashed red lines encircle areas for update at even t timesteps. Diagonal, dashed lines are parallel with the x and y axis and are projection of the octahedron edges.

ing laws were performed [5]. For example in case of the interface width growth we used

$$\beta_{\text{eff}} \left(\frac{t_i - t_{i/2}}{2} \right) = \frac{\ln W(L \rightarrow \infty, t_i) - \ln W(L \rightarrow \infty, t_{i/2})}{\ln(t_i) - \ln(t_{i/2})} \quad . \quad (20)$$

In our studies the simulation time, measured in Monte Carlo steps (MCS), between two measurements was increased exponentially

$$t_{i+1} = (t_i + 10)e^m \quad , \quad (21)$$

using $m = 0.01$ and $t_0 = 0$. Statistical uncertainties are provided as 1σ -standard errors, defined as $\Delta_{1\sigma}x = \sqrt{\langle x^2 \rangle - \langle x \rangle^2} / (N - 1)$.

Throughout this study we used the implementation of the Levenberg–Marquadt algorithm [41, 42] in the gnuplot software [43] for non-linear least squares fitting.

For $p = q > 0$ the octahedron model describes the surface growth of the EW equation [32] in $2 + 1$ dimensions. In this case the autocorrelation function of heights has been derived [44, 45]:

$$C_h^{\text{EW}} = c_0 \ln \left(\frac{t+s}{t-s} \right) \quad , \quad (22)$$

where c_0 is a model-dependent constant. This function approaches 0 for $t \gg s$ as a power law (PL) with the exponent $\lambda_{C,h,\text{EW}}/z_{\text{EW}} = 1$, where $z_{\text{EW}} = 2$. In Sect.III B 2 we shall reproduce this result numerically as a test of our simulations.

III. RESULTS

Extensive dynamical simulations were performed using both RS and SCA updating schemes. To avoid finite-size effects we considered large systems with lateral sizes of $L = 2^{16}$. Using parallelized RS simulations with DD, denoted as DTrDB, raises the question whether the results depend on the chosen domain sizes. This is addressed here by presenting results for two different DD configurations, denoted as TC=1,1 and TC=2,2. Domains contain 8×8 sites in the first case and 16×16 in the second. In both cases the probability for particle deposition is $p = 1$.

In SCA simulations the deposition probability must be $p < 1$ in order to allow stochastic noise. We investigated three cases: $p = 0.5, 0.75$ and 0.95 in depth. While KPZ runs were performed without removals: $q = 0$, in the EW growth we applied $p = q = 1$ for RS and $p = q = 0.5$ for SCA.

The roughness scaling of the interface width is analyzed in section III A. This is followed by autocorrelation and aging studies of the height as well as lattice-gas variables in section III B.

A. Roughness scaling

To compare numerical results coming from different updates we determined experimentally a scaling function $f(t, p)$, that provides collapses of $W(L, f(t, p))$ for different dynamics. In case of RS dynamics this function is linear $f_{\text{RS}}(t, p) \propto p$. Since the $p \rightarrow 0$ limit of the SCA corresponds to RS updating, we tried to extend the linear form analytically. A smaller survey study of SCA for a larger number of different $p \leq 0.95$ values was used to obtain this function numerically and resulted in the following nonlinear extension:

$$f_{\text{SCA}}(t, p) = \tilde{t}(p) = t \cdot p e^p. \quad (23)$$

The speedup with respect to linear function of RS can be understood as follows. A dimer, that was moved at a given timestep becomes the target of another update at the next sub-lattice step in the $p \rightarrow 1, q = 0$ case. This is more effective than random sequential updating. Therefore, the roughness of the KPZ grows faster than in case of RS dynamics. One can test this function by observing a reasonably collapse on Fig. 2(a) for different p -s of SCA as compared to the RS results.

Figure 2(b) shows the effective scaling exponents of β (20) for SCA and RS simulations as the function of the rescaled time variable. Most notably, the β_{eff} exponent results exhibit slightly shifted plateaus for almost two decades in time, but the difference lies well within the error-margin of our best published result $\beta_{\text{eff}} = 0.2415(15)$ [46].

a. Random-sequential The pronounced plateau visible for DTrDB, TC=2,2, suggests that corrections at these late times are small. Simple averaging of the

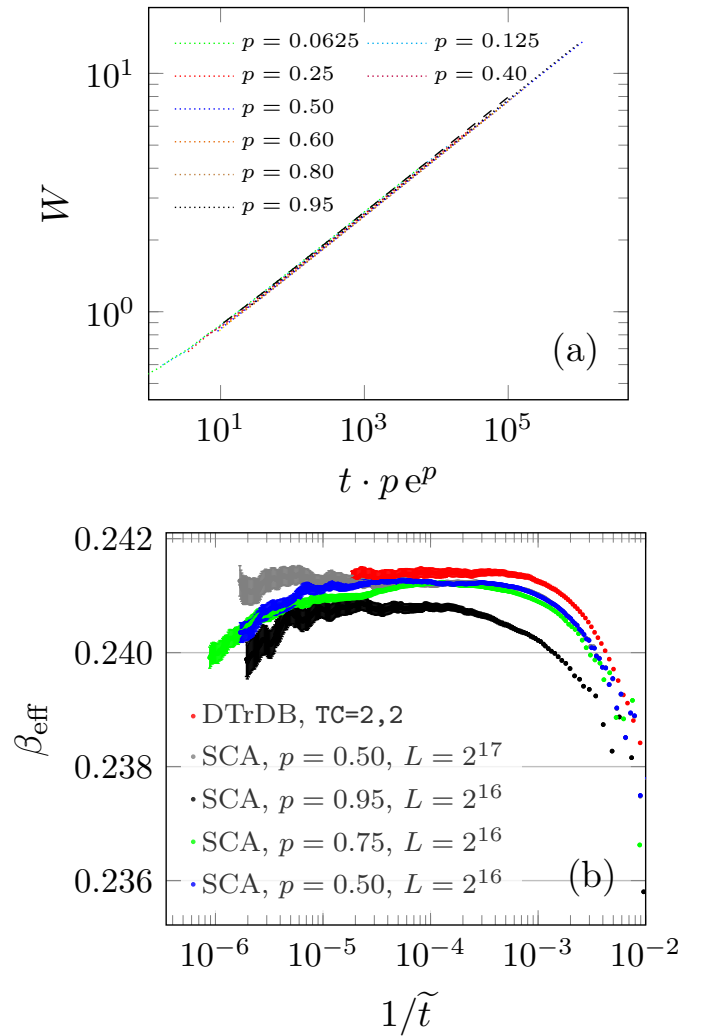


FIG. 2: Width-scaling under SCA dynamics. (a) Width curves collapsed over p by rescaling time as $\tilde{t} = t \cdot p e^p$. For comparison the DTrDB TC=2,2 result is also shown (black dashed line). (b) Effective scaling exponents under SCA dynamics for $p = 0.95$ ($n \geq 2254$), $p = 0.75$ ($n \geq 6430$) and $p = 0.5$ ($n \geq 373$, $n \geq 3062$). RS data is shown for comparison ($n \geq 708$). Propagated 1σ error bars are attached to the effective exponents, merging into an error-corridor at late times due to the dense placing of points.

plateau values, yields $\beta_{\text{DTrDB,TC=1,1}} = 0.24146(1)$ and $\beta_{\text{DTrDB,TC=2,2}} = 0.24139(1)$. The case TC=1,1 was excluded from figure 2(b) to reduce cluttering. It is presented separately in figure 4(a) and shows slightly stronger corrections, which we ignored by assuming a constant plateau. This causes slightly different average values and uncertainty beyond the pure statistical error. Therefore, we provide the unified estimate $\beta = 0.2414(2)$, with an error margin of about the same size as the 1σ -error bars attached to the effective exponents at late times.

b. Stochastic cellular automaton Like in the RS case, there is a plateau spanning almost two decades

in the $L = 2^{16}$ datasets, suggesting significantly different scaling exponents, which depend on p : $\beta_{p=0.95} = 0.24079(1)$ and $\beta_{p=0.5} = 0.24122(1)$. While the latter falls within the error margin of the value derived from RS runs, the former does not. The spread of these values $\Delta\beta_{\text{SCA}} = 0.00043(2)$ is marginally significant, even though corrections have not been considered. The effective exponents of the SCA runs with $p = 0.75$ show intermediate behavior: while they are close to $\beta_{\text{eff},p=0.5}(1/\tilde{t})$, they tend downward after $1/\tilde{t} \gtrsim 1 \times 10^{-4}$ and approach the curve $\beta_{\text{eff},p=0.95}(1/\tilde{t})$.

The possibility, that SCA simulations exhibit different growth exponents depending on $p < 1$ raises doubts about correct modelling KPZ surface growth. In this case, the asymptotic scaling exponents obtained by SCA would differ from the actual KPZ value and converge only in the RS-limit $p \rightarrow 1/V$. The plots also show a break down of β_{eff} at late times. Such behavior can be attributed to the onset of the steady state, which seems to be unlikely: $\xi \propto t^z \sim L$ would be reached about one decade later than the left end of the displayed plot. Another explanation might be the possibility of blockades in the dimer lattice-gas due to the correlated updates, which start to move through the system as waves, and slow down the growth of surface roughness. This effect can depend on p , but should be independent of L , except for very small systems, where real finite size effects set in before the wave phenomenon could be observed. The presented data suggest scaling of this cut-off with p , because the kink appears at about the same rescaled time $\tilde{t} \approx 1.7 \times 10^5$ MCS in all SCA simulations of size $L = 2^{16}$.

Most importantly, the β_{eff} curve does not exhibit cut-off in the plateau in case of our largest sized $L = 2^{17}$ data, but matches perfectly the RS result. It only shows noise related oscillations within the 1σ -error margin. This indicates that the cut-off is related to finite sizes that will be investigated further in the following section.

1. Distribution of interface heights in the growth regime

In order to get information about the shapes of the distribution of the SCA interface heights we calculated their lowest moments. Fig. 3 shows the evolution of the cumulant ratios S and Q , defined by equations (8) and (9). The curves approach their growth regime asymptotic values, but move away again at late times. These values: S_∞ and Q_∞ can be determined by performing a fit of the form

$$R(t) = R_\infty + b_R \cdot \tilde{t}^{c_R} \quad , \quad (24)$$

where R is a placeholder for S or Q , in the interval: $200 \leq \tilde{t} \leq 200\,000$ MCS, which excludes early time oscillations as well as the cut-off at late times, coming from $\xi \rightarrow L$. This yields $S_{\text{h,growth}} = -0.427(2)$ and $Q_{\text{h,growth}} = 0.351(3)$, in agreement with literature values [47, 48] for the KPZ universality class. The sign of

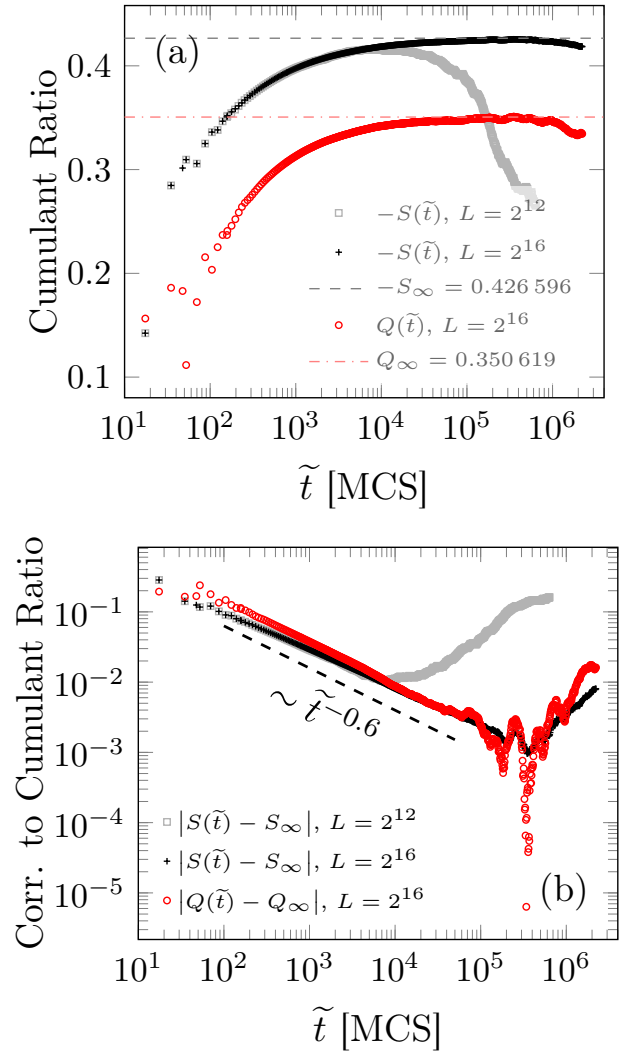


FIG. 3: Skewness S and kurtosis Q of the distribution of interface heights in the growth regime. The data belongs to the set of SCA runs with $p = 0.75$, $L = 2^{16}$ ($n_{\text{SCA},p=0.75} \geq 6430$, compare figure 2). The skewness for a smaller dataset for $L = 2^{12}$ ($n_{\text{SCA},p=0.75,L=2^{12}} \geq 45$) is included to illustrate finite-size behavior. (a) Cumulant ratios as functions of time. The horizontal lines show the obtained fit parameters for the asymptotic values, to guide the eye. See text for proper values with error estimates. (b) Finite-time and finite-size corrections to the asymptotic values of the cumulant ratios.

S depends on the choice $p \gtrless q$ in the simulations, corresponding to $\text{sign}(\lambda)$ of the KPZ equation (1). Panel (b) of Fig. 3 shows the deviations from these asymptotic values. The error estimates given above originate from this representation: The error is assumed to be by the order of the closest approach of the numerical data to the asymptotic value. Exponents of (24) are $c_S \approx -0.54$ and $c_Q \approx -0.60$. The value $c_R \approx -0.6$ also holds for a number of other dimensionless cumulant ratios, not displayed here.

After the closest approach to the asymptotic values

in the growth regime, $S(\tilde{t})$ and $Q(\tilde{t})$, both, move in the direction of their respective values in the steady state: $S_{h,\text{steady}} \approx 0.26$ and $Q_{h,\text{steady}} \approx 0.13$ [37, 49, 50]. The shape of the distribution of surface heights changing in this way is an indication of finite-size effects becoming relevant at $\tilde{t}_{\text{fs}} \approx 3 \times 10^5$ MCS. This coincides with the time at which the cut-off [66] in $\beta_{\text{eff}}(\tilde{t})$ was observed in SCA runs for $L = 2^{16}$ (see Fig. 2(b)). Hence it becomes clear, that this change in β_{eff} is caused by finite-size effects. In Fig. 3(b) we also plotted $S(\tilde{t})$ of a smaller system, for which the steady state is reached at $\tilde{t} < 4 \times 10^5$ MCS $\simeq 2^{12z}$.

2. KPZ ansatz for the growth regime

Analytical and numerical investigations of KPZ models in 1 + 1 dimensions found that finite-time corrections to $h(t)$ took the form $\propto t^{-\beta}$ for the interface height [22, 51–53]:

$$h(t) = \text{sign}(\lambda) \cdot (\Gamma t)^\beta \chi + \xi + \zeta t^{-\beta} \quad ,$$

where λ , Γ , ξ and ζ are model-dependent parameters and χ is a universal random variable with GOE distribution in case of a flat initial condition. The KPZ ansatz hypothesis states, that a generalisation of this form should also hold in higher dimensions [47, 48], leading to the following ansatz for the effective growth exponent of the height:

$$\beta_{\text{eff},h} = \beta + \sum_{n=1}^N c_n t^{-n\beta} \quad , \quad (25)$$

with non-universal parameters c_n and N . Higher moments of the height $\langle h^n \rangle$ show corrections $\propto t^{-n\beta}$, accordingly, and thus $\propto t^{-2\beta}$ for the roughness, prescribing:

$$\beta_{\text{eff}} = \beta + \sum_{n=1}^N c_n t^{-2n\beta} \quad (26)$$

In the 2 + 1 dimensional restricted solid-on-solid model (RSOS) model, the dominant corrections to the roughness growth were found to be of order $\propto t^{-4\beta}$ [48], which motivates the inclusion of higher orders in these forms. Ideally, such a model would fit the data well as soon as all relevant orders are included. Adding more terms should not improve the fit quality further. However, with noisy data, adding more free parameters in this way, can result in over fitting, if not convergence-problems.

Fig. 4 shows fits results using equation (26) on the previously introduced datasets. It is immediately apparent, that (26) with $N = 1$ does not describe the presented data, the $n = 2$ -term is required, as in case of the RSOS model.

In case of RS simulations, the ansatz appears to fit reasonably well early times: $\tilde{t} \geq 100$ as well. The SCA

runs on the other hand show strong oscillations at early times, caused by the synchronous updates and are not expected to be described by the KPZ ansatz. Still, late times, in the interval $1 \times 10^{-5} \leq 1/\tilde{t} \leq 3 \times 10^{-3}$, can be fitted well by (26). The case $p = 0.75$ poses some exception here, due to its non-monotonous characteristics in the apparent cross-over from $p = 0.5$ -like to $p = 0.95$ -like behavior.

A more quantitative summary is provided in Tab. I, which lists the reduced sums of residuals χ_{red} to quantify agreement between the fitting model and the data. Eq. (26) describes all datasets the best, if two terms $\propto \tilde{t}^{-2\beta}$ and $\propto \tilde{t}^{-4\beta}$ ($N = 2$) are included, except SCA with $p = 0.75$, which requires more free parameters to approximate it's more complicated form at late times.

Where the KPZ ansatz does indeed apply, fits of the more general models (25) should not show increased agreement with the data. The table shows them to be less consistent with respect to the resulting estimates for β . They provide the best description of the data with only the term $\propto \tilde{t}^{-2\beta}$, but one or two additional *odd* terms present ($N = 2, 3$). The best fits resulting from models (26) are consistently better than those of (25), across all datasets, which justifies discarding the latter class of models and thereby supports the KPZ ansatz hypothesis.

To obtain estimates of β for each dataset, the best-fit value was used. The β spread values for higher N , provide an estimate for over fitting and may serve as an error estimate for a small confidence interval of 1σ . For simulations with RS dynamics, this yields $\beta = 0.2414(2)$, which is remarkably identical to the result based on an average of the late-time plateau of β_{eff} .

The estimates obtained this way may be less reliable for SCA datasets, because here the model can only fit a fraction of the available time series which must exclude the initial oscillations. It can be noted, that the $\beta_{p=0.5} = 0.2411(2)$ is basically the same as the one obtained before. For large p the estimate $\beta_{p=0.95} = 0.2409(4)$ agrees with the previous one as well as, marginally, with the one from RS runs. However, this result is obtained because, the model predicts the effective exponents to move upwards for $\tilde{t} \rightarrow \infty$. This prediction should be regarded with care, since it remains unclear how far the KPZ ansatz could be applied for $p \rightarrow 1$. For $p = 0.75$ we refrain from making an estimate, because the model does not seem to describe the data well.

3. The KPZ dynamical exponent

The dynamical exponent $z = \alpha/\beta$ of the KPZ class is related to the roughness exponent α by the Galilean symmetry [12]:

$$2 = \alpha + z = \alpha(1 + 1/\beta) \quad . \quad (27)$$

Inserting the our estimate $\beta = 0.2414(2)$ into this equation yields $\alpha = 0.3889(3)$ and $z = 1.611(3)$. The latter is used to calculate autocorrelation exponents in the

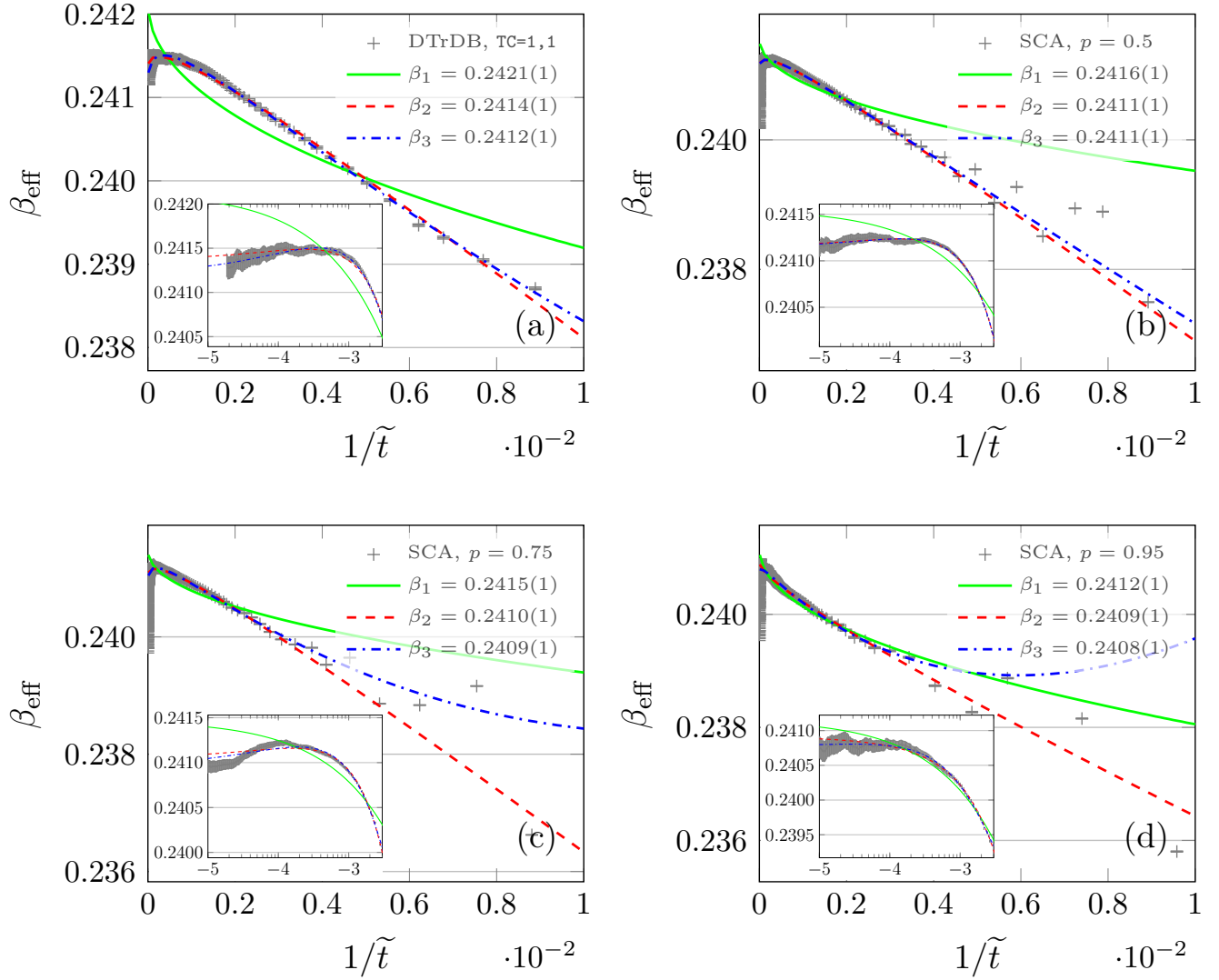


FIG. 4: Effective exponents β_{eff} for roughness growth with KPZ ansatz fits using the form (26) to orders one through three. The resulting asymptotic values for β are given in the legends accompanied by the uncertainty of the fit parameter. The insets show a zoom to the late-time region $1 \times 10^{-5} \leq 1/\tilde{t} \leq 3 \times 10^{-3}$ (truncated before the finite size break down Fig. 2(b)). The $1/\tilde{t}$ axes are logarithmically scaled using base 10, the labels only show the exponents. Panel (a) shows the RS dataset using DTrDB with $\text{TC}=1,1$. Fits were performed in the interval $1 \times 10^{-5} \leq 1/\tilde{t} \leq 1 \times 10^{-2}$. Panels (b)-(d) show SCA datasets with $p = 0.5, 0.75$ and 0.95 , respectively. The fits were restricted to the interval shown in the inset. The sample size for DTrDB, $\text{TC}=1,1$ was $n \geq 1044$. See the captions of Fig. 2 for other sample sizes.

next section. It should be noted, that the above value for α , while in agreement with earlier numerical estimates [37, 46, 54, 55], marginally disagrees with the currently most accepted one $\alpha = 0.3869(4)$ [56]. Combining this roughness exponent results with our own estimate for β violates equation (27) by about 2.5σ . This may be marginal, but still, we use our α and z estimates for consistency.

B. Autocorrelation

1. Autocorrelation of interface heights in the KPZ case

a. Aging The autocorrelation results of the interface heights under RS dynamics are summarized in Figure 5. A near-perfect collapse of the $C_h(t, s)$ functions could be achieved by using b from the relation (14) (see Figure 5(a)). However, the best collapse was obtained with the following aging exponent: $b_h = -0.469(3)$. This is the consequence of strong corrections to scaling at early times, where $\beta_{\text{eff}}(t)$ is smaller than the asymptotic value

TABLE I: Summary of fitting of β_{eff} using the KPZ ansatz in the most general form (25) and using (26) with even powers, more suitable to describe corrections of the roughness-scaling up to maximum orders $N = 6$. Error margins given are uncertainties of the fit parameters, not actual error estimates for β . The reduced sums of residuals χ_{red} are given to judge the quality of the fits. For each dataset we underlined the value of χ_{red} , where the quality does not improve significantly by increasing N .

N	RS				SCA					
	DTrDB, TC=1,1		DTrDB, TC=2,2		$p = 0.5$		$p = 0.75$		$p = 0.95$	
	β	χ_{red}	β	χ_{red}	β	χ_{red}	β	χ_{red}	β	χ_{red}
equation (25)										
1	0.2430(1)	10.04	0.2433(1)	9.24	0.2420(1)	7.03	0.2419(1)	8.63	0.2418(1)	3.15
2	0.2396(1)	1.82	0.2396(1)	<u>1.29</u>	0.2403(1)	1.62	0.2400(1)	1.31	0.2403(1)	<u>0.51</u>
3	0.2411(1)	<u>0.79</u>	0.2408(1)	0.55	0.2414(1)	<u>0.64</u>	0.2404(1)	<u>1.18</u>	0.2401(1)	0.49
4	0.2421(2)	0.67	0.2421(1)	0.32	0.2414(1)	<u>0.64</u>	0.2385(1)	0.63	0.2403(2)	0.48
5	0.2386(3)	0.47	0.2409(2)	0.28	0.2388(3)	0.51	0.2394(3)	0.61	0.2399(5)	0.48
6	0.2377(8)	0.47	0.2403(5)	0.28	0.2333(9)	0.45	0.2420(7)	0.59	0.2485(8)	0.40
equation (26)										
1	0.2421(1)	7.28	0.2422(1)	6.27	0.2416(1)	5.22	0.2415(1)	6.54	0.2412(1)	1.76
2	0.2414(1)	<u>1.16</u>	0.2414(1)	<u>1.10</u>	0.2411(1)	<u>0.65</u>	0.2410(1)	1.72	0.2409(1)	<u>0.81</u>
3	0.2412(1)	0.65	0.2412(1)	0.33	0.2411(1)	0.64	0.2409(1)	1.51	0.2408(1)	0.52
4	0.2413(1)	0.53	0.2412(1)	0.29	0.2412(1)	0.59	0.2407(1)	<u>0.86</u>	0.2407(1)	0.50
5	0.2412(1)	0.51	0.2412(1)	0.28	0.2412(1)	0.59	0.2406(1)	0.68	0.2405(1)	0.41
6	0.2412(1)	0.51	0.2412(1)	0.28	0.2411(1)	0.57	0.2403(1)	0.50	0.2407(1)	0.38

(see Figure 2(b)).

b. Autocorrelation exponent obtained by RS dynamics We calculated effective exponents of $\lambda_{C,h}/z$ and its $t/s \rightarrow \infty$ behavior, by an analysis shown on Figure 5(b). In order to read-off the appropriate correction to scaling we linearised the left tail of the curves by plotting them on the $\sqrt{s/t}$ scale. This leads to the extrapolations $\lambda_{C,h}/z = 1.254(9)$ depending on s . The aging behavior should be independent of s , but corrections arising at finite s values can affect the extrapolation results. This is demonstrated on Figure 5(c). The plot suggests a rough asymptotic trend of decreasing effective exponents, but does not allow one to make a clean fit.

To clarify the situation we attempted a different type of local slope analysis presented in Figure 5(d), using tail effective exponents, where each $\lambda_{C,h}/z$ value was determined as the exponent of a PL-fit to $C_h(t', s)$ for $t' \geq t$. These can be expected to converge more monotonically to the asymptotic value as before, because the left tail data of $C_h(t, s)$ are included in the procedure for all t_{\min} with an increasing weight as t_{\min} increases. Indeed, the curves of different s values in Figure 5(d) behave more linearly with some additional oscillations. However, all curves seem to fluctuate around a common mean, which is not the case in Figure 5(b). A single linear fit for the combination of all curves, yields an averaged extrapolation of $\tilde{\lambda}_{C,h}/z = 1.23(3)$ in a marginal agreement with our previous result for this $\lambda_{C,h}/z = 1.21(1)$ [39]. The present larger error margin takes the uncertainty due to the actually unknown corrections into account. Using our z value the corresponding autocorrelation exponent is $\lambda_{C,\text{heights}} = 1.98(5)$. Figure 5 mostly shows data for

simulations using DTrDB, TC=1,1; the above estimates are also compatible with results obtained using TC=2,2; as evidenced by figure 5(c).

c. SCA autocorrelation functions and aging SCA updates are spatially correlated, therefore they introduce a contribution to the autocorrelation function, which depends on the update probability $p < 1$. If we want to model cellular automaton like systems this is not a problem, but for describing the KPZ equation this is artificial. Figure 6 compares the autocorrelation functions of height variables at $p = 0.95$ and $p = 0.5$. The most apparent property is the finite asymptotic value (Figure 6(a)). This is the consequence of frozen regions, arising in ordered domains, which are difficult to randomize by the SCA dynamics. In the dimer model updates can happen at the boundaries only, besides this alternating domains are also stable in case of SCA, they flip-flop at even-odd sublattice steps, when $p \rightarrow 1$.

We applied an iterative fitting procedure to determine the functional behavior as follows. As a first approximation the $C_h(t \rightarrow \infty, s, p) = o(p)$ limit was determined using a linear extrapolation from the function's right tail. Subtracting the appropriate value from each curve revealed a PL approach to this constant. To obtain refined $o(p)$ values, the exponent x was read off from the data, allowing a subsequent fit for the tail in the form:

$$f(t) = o + c \cdot t^{-x}, \quad (28)$$

with free parameters o and c . The corrected exponents converged as $x' \rightarrow \lambda_C/z$, after subtracting the refined $o(p)$ values. These iterations yielded self-consistent estimates for $o(p)$ and the autocorrelation exponent of the

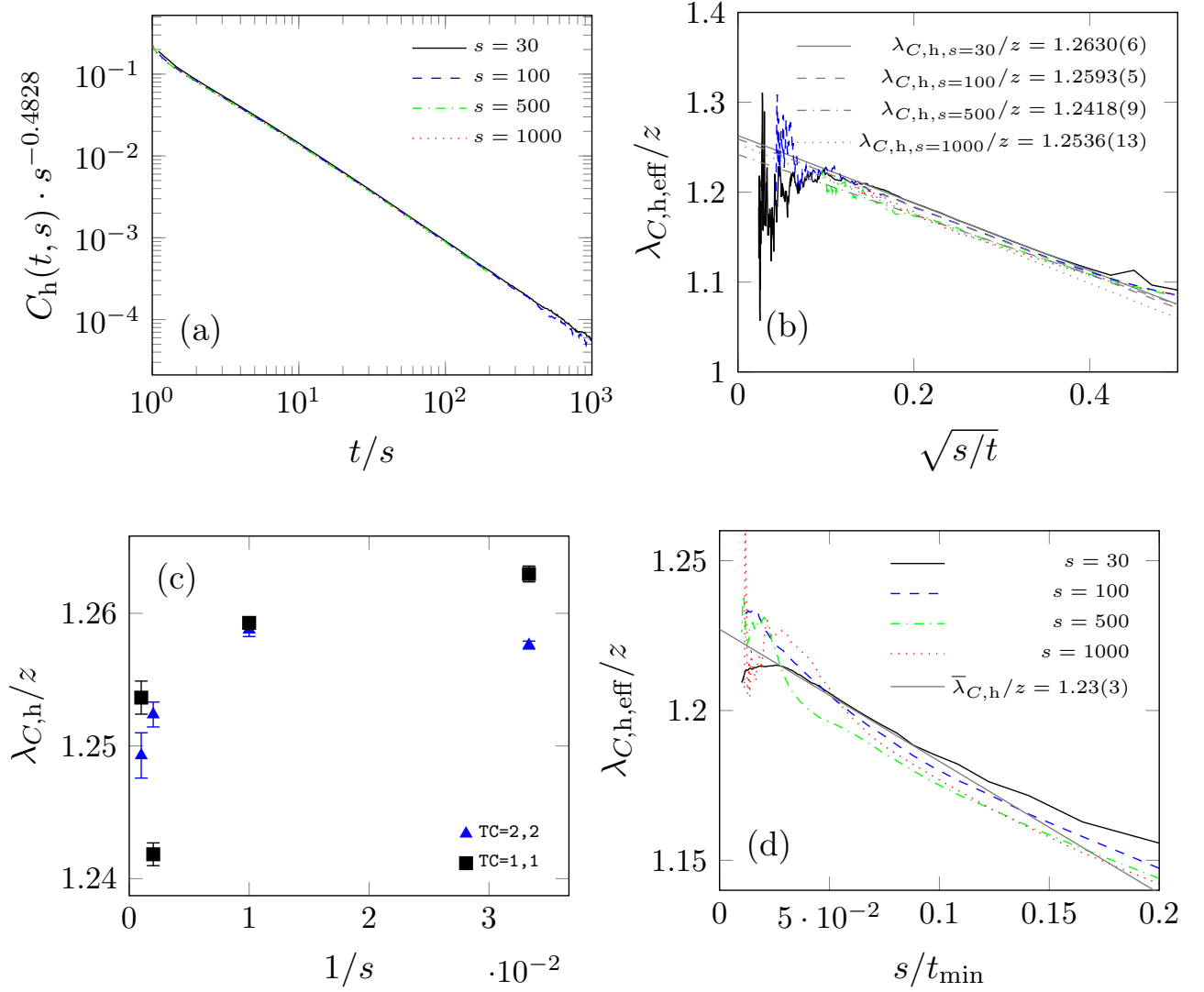


FIG. 5: Autocorrelation results from RS calculations using DTrDB with TC=1,1. System size $L = 2^{16}$, $n \geq 1044$ realizations for $s > 30$ and $n \geq 473$ for $s = 30$. (a) Collapsed autocorrelation functions for waiting times $s = 30, 100, 500, 1000$. (b) Corresponding local slope analysis and extrapolations assuming corrections of the form $\sqrt{s/t}$, as drawn. Linear fit was performed for $\sqrt{s/t} \in [0.1, 0.3]$. Stated errors are pure fit-errors, see text for actual error margins. (c) Exponents $\lambda_{C,h}/z$ as obtained in panel (b), corresponding values obtained in DTrDB TC=2,2 simulations are displayed additionally. (d) Tail effective exponents corresponding to panel (a) obtained from PL fits for intervals $t \geq t_{\min}$ with successively increasing t_{\min} . A linear fit to the combination of all curves is displayed as a solid black line.

SCA. This procedure is more prone to statistical error for small t/s , because $C_h(t, s)$ is farther away from the asymptotic behavior in this case, allowing noise in the tail to influence the extrapolated value more strongly. Table II lists the calculated $o(p)$ limits (including those for the lattice-gas variables, see Section III B 3).

The limiting value turned out to depend exponentially on p . Note, that similar e^p dependence has been found in $f_{\text{SCA}}(t, s)$ relating SCA and RS timescales [67].

Figure 6(b) shows the corrected $C_h(t, s)$ functions, after subtracting the limiting $o(p)$ values. A nearly perfect data collapse could be achieved using the aging exponent b_h , coming from the RS simulations. Even more,

the corrected SCA and the displayed RS autocorrelation functions show identical behavior.

d. Autocorrelation exponent: SCA Local slope analyses of the corrected autocorrelation functions are displayed in figures 6(c) and 6(d) at $p = 0.95$ and $p = 0.5$, respectively. Assuming a rescaling of the abscissa: $\sqrt{s/t}$, allows one to observe a linear behavior of the effective exponents for intermediate times. In case of $p = 0.95$ the o -values could not be determined precisely enough for $s > 100$, thus we considered extrapolations at $s = 30, 100$ only in a weighted average of the results. This yielded: $\lambda_{C,h}/z = 1.26(1)$ and so $\lambda_{C,h} = 2.01(2)$. These values

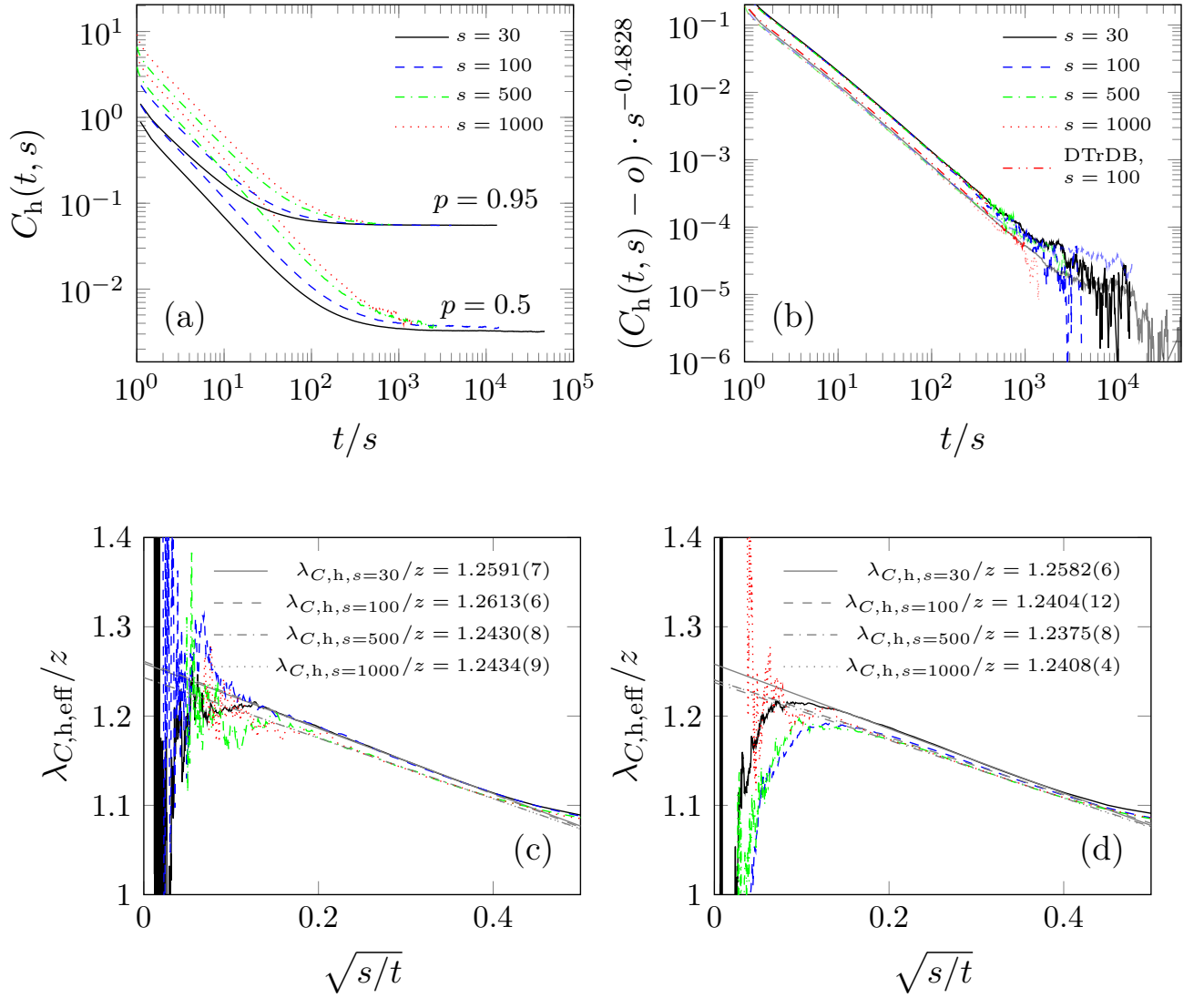


FIG. 6: Autocorrelation of KPZ heights from SCA calculations. Error bars have been omitted for clarity. The visible noise is a good indication for 1σ error. Panels (a) and (b) show data sets with $p = 0.5$ (3062 realizations, $t \leq 1.4$ MMCS) and $p = 0.95$ (3062 realizations, $t \leq 400$ KMCS), curves from bottom to top. Lateral system size is $L = 2^{16}$. (a): Raw autocorrelation functions showing saturation depending on p . (b): Collapsed autocorrelation functions, corrected by the saturation offset o (see text). Plots for $p = 0.5$ and $p = 0.95$ corresponding to the same s use the same colors, where the bottom set of plots corresponds to $p = 0.5$. Colors are less saturated for the plots for $p = 0.5$, to distinguish them at late times. The DTrDB, TC=1,1 autocorrelation function of $s = 100$ is also displayed for comparison. The bottom panels (c) and (d), show the local slope analysis corresponding to the $p = 0.95$ and $p = 0.5$ data sets, respectively. Extrapolations assume corrections of the form $\sqrt{s/t}$, as drawn. Printed error margins are pure fit-errors.

are in good agreement with those obtained from a local slope analysis of RS calculations for small s .

The effective exponents for $p = 0.5$ show a slightly decreasing tendency with s in Figure 6(d), moving towards the RS estimate $\tilde{\lambda}_{C,h}/z = 1.23(3)$. However, we can't consider the extrapolated values for $s = 500$ and $s = 1000$ more precise, than those at $s = 30, 100$, because the determination of the $o(s)$ constant becomes more uncertain at higher times, increasing the possible error of the exponent estimates.

2. Autocorrelation of interface heights in the EW case

Since the autocorrelation function in the EW case is known exactly (22), we can verify our simulations by a comparison with it. Indeed, the expected form could be reproduced by our RS implementation. A more interesting result is, that the SCA simulations also fit it perfectly. The finite saturation value, caused by correlated updates, observed in the KPZ case is not present here.

The agreement with the analytical form is exemplified in Figure 7(b). A small deviation at very early times can

TABLE II: Autocorrelation limits for KPZ with SCA dynamics for different deposition rates p and $q = 0$, as functions of the waiting time s . Fit errors are shown, which are below the given number of digits in case of the slopes.

s/MCS	o_h		o_s	
	$p = 0.5$	$p = 0.95$	$p = 0.5$	$p = 0.95$
30	0.003 20(3)	0.055 398(8)	0.012 871	0.221 623
100	0.003 31(5)	0.055 20(3)	0.014 286	0.219 827
500	0.0031(2)	0.054 57(8)	0.013 944	0.218 547
1000	0.0035(3)	0.0548(2)	0.013 903	0.218 330

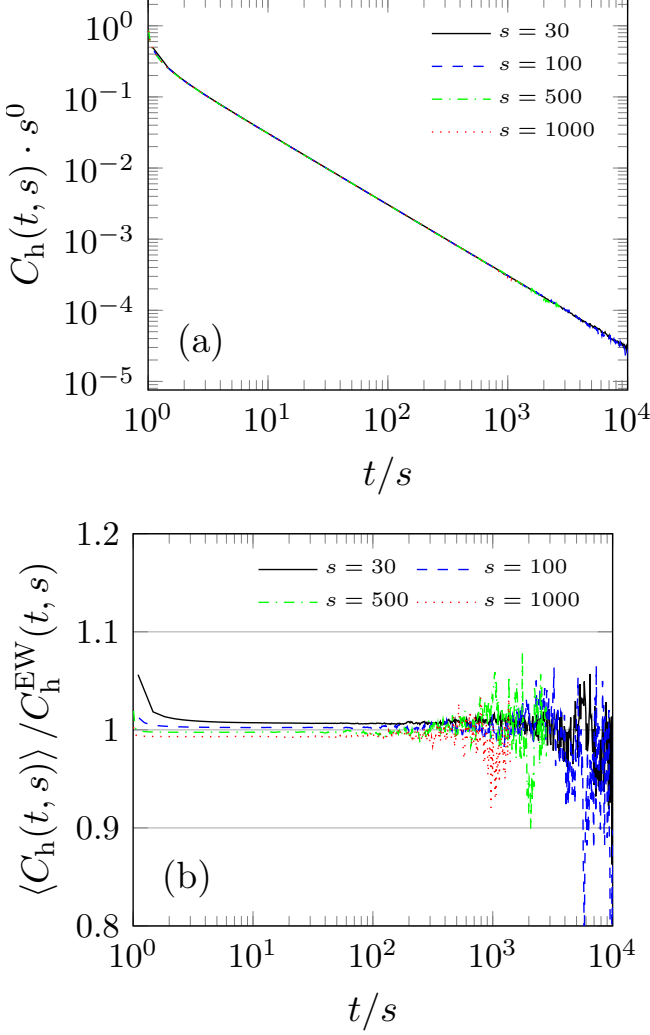


FIG. 7: Autocorrelation functions of heights under SCA dynamics with $p = q = 0.5$ (EW). Sample size is $n_{\text{SCA}} = 5919$. Error bars are omitted for clarity. The magnitude of fluctuations can be seen from the visible fluctuations in the plots. (b) The same data divided by C_h^{EW} .

be observed here, as well as in the RS results and should be related to the initial conditions of the simulation with respect to those of the analytical calculations. The application of a fit with (22) results in $c_0 \simeq 0.152$ for different

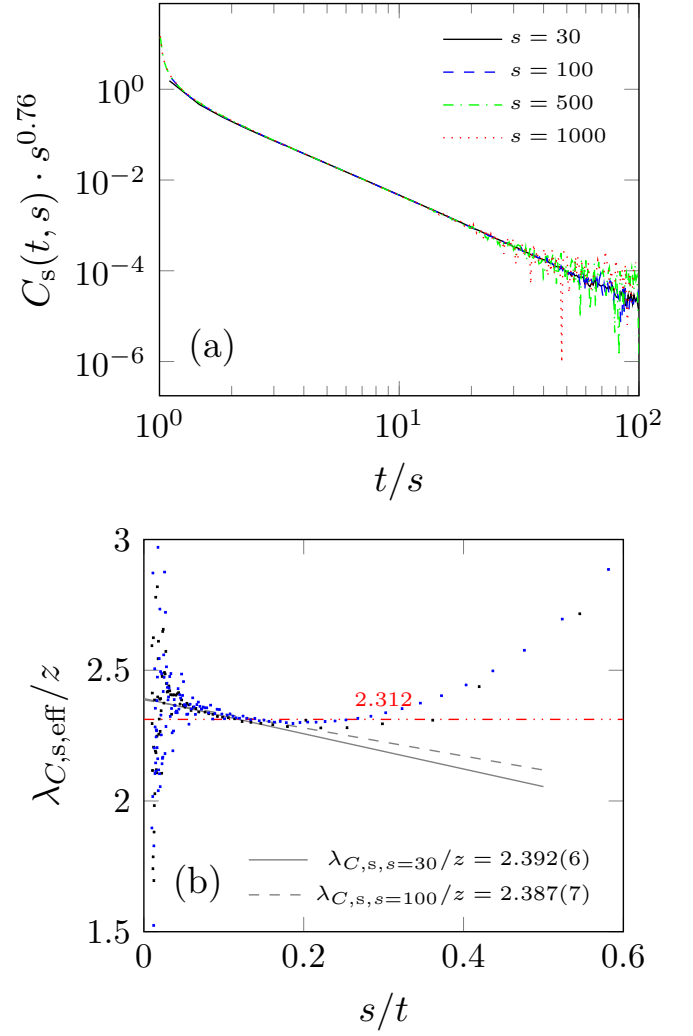


FIG. 8: Autocorrelation results from RS calculations using DTrDB with $\text{TC}=1,1$ (the same runs as those shown Figure 5). (a) Collapsed autocorrelation functions for $s = 30, 100, 500, 1000$. (b) Local slope analysis for $s = 30, 100$. Linear fitting lines are also shown, assuming corrections of the form s/t in the interval $t/s \in [6.25, 50]$. The horizontal line (---) marks the value obtained from direct PL fits.

waiting times s . Using the consistency relation (14) for $s \rightarrow t$ we can expect the same value, which was derived for the octahedron model in [32] for the $s \rightarrow \infty$ limit.

These numerical results do not only show the correctness of the SCA and RS implementations of the roughening kinetics, but provide an example, where the correlations introduced by SCA do not affect the dynamical behavior.

3. Autocorrelation of lattice-gas variables in the KPZ case

Next we show results for the lattice-gas variables corresponding to the binary slope values of heights of the KPZ growth presented earlier (see Figure 8) using RS

dynamics. Here again, the $C_s(t, s)$ functions of different waiting times collapse almost perfectly with the value: $b_s = 0.76(2)$. In a previous paper [39] we reported: $b_s = 0.70(1)$, which were obtained by a smaller sized analysis.

a. Autocorrelation exponent: RS Since the density autocorrelation functions decay much more rapidly than those of the heights, the signal-to-noise ratio in the present sample is insufficient for a reliable extrapolation based on the effective exponents. A weighted average of direct PL fits for $4 \leq t/s \leq 90$ yielded $\lambda_{C,s}/z = 2.312(2)$. However, the effective exponents show curvature as $t/s \rightarrow \infty$ and suggest an asymptotic value $\lambda_{C,s,\text{eff}}/z = 2.39(2)$. In [39] we obtained $\lambda_{C,s,\text{eff}}/z = 2.35(2)$, coming from $s = 30$, $L = 2^{13}$ sized CPU simulations.

b. SCA density autocorrelation functions Similarly to the case of interface heights the $C_s(t, s)$ functions approach finite values asymptotically, as shown in Figure 9(a) as the consequence of the SCA dynamics. The computed values of $o(p, s)$ are listed in Table II.

Figure 9(b) shows the corrected functions $C_s(t, s) - o(p)$ in comparison with our RS result. Data collapse for $p = 0.5$ and $p = 0.95$ could be achieved using the common aging exponent value $b_s = 0.76$, obtained from our previous RS calculations. This indicates, that the density correlation behavior is not changed by the application of SCA updates as in case of the height variables.

c. SCA density autocorrelation exponent: In contrast with the interface height results the density correlation exponent of the corrected $C_s(t, s)$ exhibits a more complex behavior. The dataset for $p = 0.95$ clearly exhibits a different exponent than what we observed in case of the RS simulations. We show effective exponents fitting for $s = 30$ and 100 , where the signal-to-noise ratio is better on Figure 9(c). A direct linear fit extrapolating to $s/t \rightarrow 0$ yields an estimate of $\lambda_{C,s,\text{SCA}}/z = 0.75(2)$.

At $p = 0.5$ we can find a crossover from the RS to a different, SCA asymptotic behavior in Figure 9(d). A linear extrapolation for the tail of this crossover curve results in $\lambda_{C,s,\text{SCA}}/z$, in good agreement with the $p = 0.95$. This leads to the following numerical form for the tail of the autocorrelation function under SCA dynamics:

$$f_{C,\text{SCA}}(t/s, p) \propto c_1 \cdot (t/s)^{-\lambda_{C,s}/z} + c_2 \cdot (t/s)^{-\lambda_{C,s,\text{SCA}}/z} \quad (29)$$

4. Autocorrelation of lattice-gas variables in the EW case

a. RS autocorrelation functions In case of RS simulations, the tail of $C_s(t, s)$ does not decay with a simple PL as can be observed in the Figure 10. The pronounced curvature in the log-log plot suggests a slower than PL decay at first glance. However, the effective exponents (inset) suggest a PL with an asymptotic exponent $\lambda_{C,s}^{\text{EW}}/z_{\text{EW}} = 0.7(2)$, following a cross-over from an early-time regime.

b. SCA autocorrelation functions While the SCA dynamics seems to reproduce the expected autocorrelation function of the surface heights after the removal of the constant, the evolution of the underlying lattice gas is different. In case of $p = q = 0.5$ the density autocorrelation exhibits a PL tail, characterized by $\lambda_{C,s}^{\text{SCA},0.5}/z_{\text{EW}} \approx 2$ (see inset of Figure 10).

In the $p \rightarrow 0$, $q \rightarrow 0$ limit the SCA crosses over to an effective RS dynamics, because we avoid the correlated updates of the lattices. This is indeed the case here, evidenced by the $p = q = 1/32$ results (see Figure 10). Following a rescale of time $t = p \cdot t$ one can find a good collapse with the RS results. Therefore, the update dynamics seems to affect the scaling behavior of the density autocorrelation function.

c. Aging The aging exponent obtained from the presented simulations is $b_s^{\text{EW}} = 1.1(2)$. This value holds for both RS and SCA dynamics, but breaks down for very small values of s .

IV. DISCUSSION AND CONCLUSIONS

We performed extensive simulations of the octahedron model by RS and SCA dynamics. Precise estimates were obtained for the dynamical behavior: exponents as well as probability distributions of the KPZ and EW universality classes. The main advance of this work, in the long story of KPZ research, is the influence of correlated SCA dynamics on the universal properties of these models. Furthermore, we determined the aging properties of the underlying DLGs of the octahedron model.

By determining moments of the probability distributions we could study finite size effects and arrived at the conclusion that the corrections related to this become relevant much before the occurrence of the steady state. Our surface growth simulations support the validity of the KPZ ansatz hypothesis in $(2+1)D$ and yield a growth exponent $\beta = 0.2414(2)$, from which $\alpha = 0.3889(3)$ and $z = 1.611(3)$ can be deduced. The growth exponent value lies within the error margins of [46, 57, 58], but not within those of the early landmark result of Forrest and Tang $\beta = 0.240(1)$ [59]. However, the small simulation cells used then demanded shorter simulations times, which could have lead to a smaller estimate due finite-time corrections. Under SCA dynamics marginally lower growth exponents were observed for deposition probabilities $p > 0.5$ and additional corrections to scaling caused the failure of the KPZ ansatz at early times.

Our estimate of the roughness exponent does not agree with the direct estimate $\alpha = 0.3869(4)$, obtained recently through a complex finite-size scaling analysis of the RSOS model by Pagnani and Parisi [56], which was based on SCA simulation with $p = 0.5$. Numerical differences between SCA dynamics RS might be a cause of this. However, since our estimate was derived using Eq. (27), a slight violation of the Galilean invariance, which was proposed for discrete systems [60], may also explain this

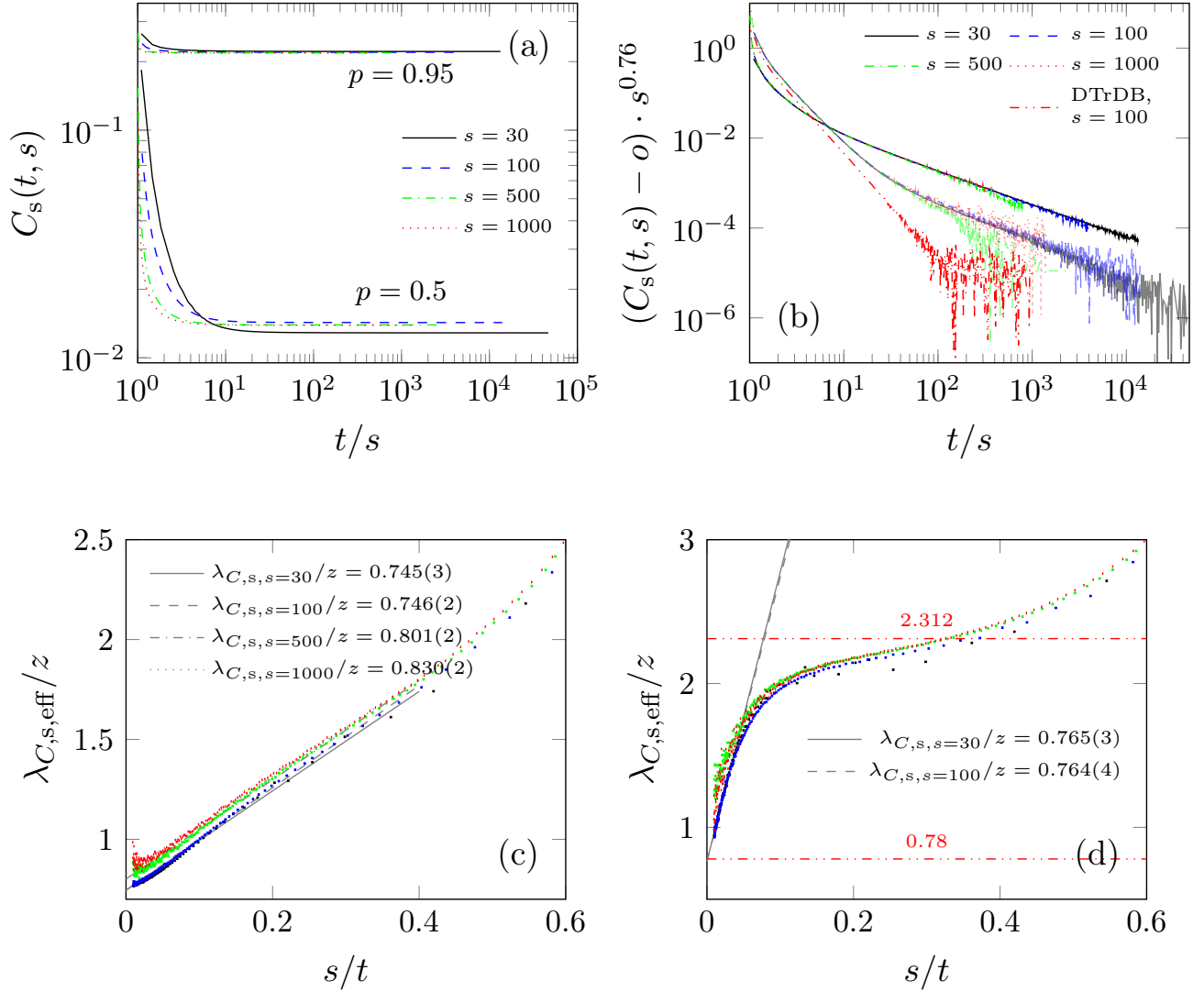


FIG. 9: Results from SCA calculations for the autocorrelation of slopes. Error bars have been omitted for clarity. The visible noise is a good indication for 1σ error. Panels (a) and (b) show data sets with $p = 0.5$ and $p = 0.95$, curves from bottom to top. Data are taken from the same runs as of Figure 6. (a): Raw autocorrelation functions showing saturation depending on p . (b): Collapsed autocorrelation functions, corrected by the saturation offset o (see text). Data from a DTrDB run for $s = 100$ is displayed in red for comparison. The bottom panels (c) and (d), show the local slope analysis corresponding to the $p = 0.95$ and $p = 0.5$ data sets, respectively. Extrapolations assume corrections of the form s/t , as plotted. Printed error margins are pure fit-errors. Horizontal lines (---) in panel (d) mark the asymptotic exponents for RS updates and SCA at $p = 0.95$, from bottom to top.

disagreement.

Both our RS and SCA simulations reproduced the expected autocorrelation behavior of interface heights in the EW universality class. In the KPZ case correlated updates resulted in $C_h(t, s)$ to approach a finite value asymptotically. However, after the subtraction of this constant we found the same universal PL tails for both types of site-selection dynamics.

In case of the underlying lattice-gas variables, we found the relevance of the SCA dynamics for the asymptotic autocorrelation decay exponents, but the aging exponent seems to be insensitive for this. Interestingly, in

case of the non-linear (KPZ) model the SCA dynamics slows the decay of the autocorrelations, while in the linear (EW) model this results in a shorter memory of the dimer model. This is the consequence of the effectivity of the ordered SCA updates, which enhances the build up (KPZ) or distortion (EW) of homogeneous areas, correlated for long times.

Our estimates for the autocorrelation exponents of the KPZ class are summarized in Table III. We provided numerical results for $C(t, s)$ in the KPZ case with unprecedented accuracy, drawn from timescales up to $t/s = 1000$ due to the high signal-to-noise ratios we could achieve by

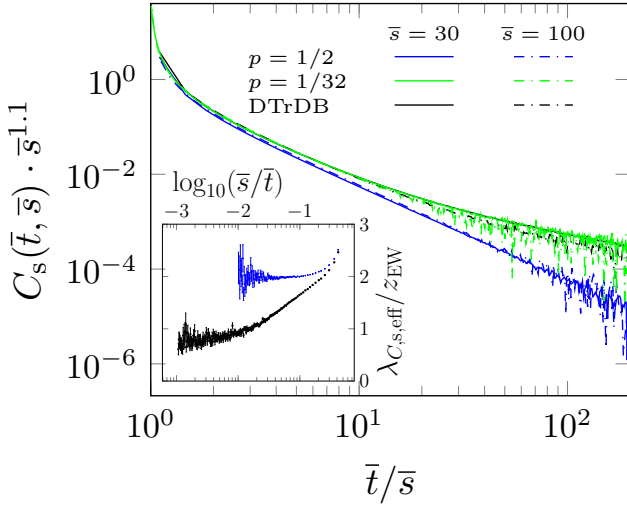


FIG. 10: Autocorrelation functions of slopes under SCA (blue and green) and RS (black) dynamics in the linear model. Sample sizes are $n_{\text{SCA},p=0.5} = 5919$, $n_{\text{SCA},p=1/32} = 147$ and $n_{\text{DTrDB}} = 2101$, for both $\bar{s} = 30$ and $\bar{s} = 100$. For SCA, $p = 1/32$, the simulation time is rescaled to collapse the curves, following: $\bar{t} = p \cdot t$, analogously for s . No rescaling is applied to the other plots: $\bar{t} = t$. Error bars are omitted for clarity. The magnitude of fluctuations can be seen from the visible fluctuations in the plots. The inset in panel (a) shows the effective autocorrelation exponents $\lambda_{C,s,\text{eff}}/z_{\text{EW}}$ for DTrDB and SCA, $p = 1/2$, both for $s = 30$ and with 1σ error bars.

TABLE III: Summary of KPZ and EW autocorrelation λ_C and aging b exponents, assuming $z_{\text{KPZ}} = 1.611(3)$ and $z_{\text{EW}} = 2$, respectively. There are no independent estimates for b under SCA dynamics. Values for the EW case provided without error margin correspond to the analytical solution [44, 45].

		$\lambda_{C,h}$	$\lambda_{C,s}$	b_h	b_s
KPZ	RS	1.98(5)	3.8(2)	-0.4828(4)	0.76(2)
	SCA	2.01(2)	1.25(2)		
EW	RS	2	1.4(4)	0	1.1(2)
	SCA	2	≈ 4		

these parallel algorithms implemented on GPUs. These simulations can be help to test predictions of theories like local scale-invariance with logarithmic corrections [30].

The KPZ autocorrelation exponent in $(1+1)$ dimensions was derived analytically $\lambda_{C,h}^{\text{d}} = 1$ [24, 25]. Later Kallabis and Krug conjectured, that in higher dimensions $\lambda_{C,h} = D$ [27] applies, but rigorous proof is still missing. Our estimates for $\lambda_{C,h}$, summarized in Table III, support this hypothesis within error margin both for RS and SCA dynamics.

We have also tested the validity of the (16) relation by Krech with our numerical data. The value for the short time dynamical exponent: $\theta = \lambda_C/z + 2\beta = 1.23(2) + 0.2414(2) \simeq 1.71(3)$ agrees well with: $(D+4)/z - 2 = 6/1.611(3) - 2 \simeq 1.72(1)$, therefore we can support the validity of the relation obtained by a perturbative RG

analysis [24, 25].

We can also compare the present estimates with our recently published values for the autoresponse $\lambda_R = 2.00(6)$ and the corresponding aging exponent $a = 0.24(2)$ [29]. $\lambda_C \simeq \lambda_R$ seems to hold within error margins. In $(1+1)$ dimensions an exceptional fluctuation-dissipation relation (FDR) exists [12, 61]:

$$T\chi(t, s; r) = -\partial_r^2 C(t, s; r) \quad . \quad (30)$$

This implies the exponent relations $\lambda_C = \lambda_R$ and

$$1 + a = b + 2/z \quad (31)$$

confirmed by simulations [62]. Our $(2+1)D$ results support the first one, but the latter is not satisfied by our numerics:

$$1 + a = 2(\beta + \beta/\alpha) \\ 1.24(2) \neq 1.724(3)$$

This calls for the existence of a possible FDR in higher dimensions. For example the generalized form

$$1 + a + (D-1)/2 = b + 2/z \quad (32)$$

is satisfied by the exponents within error limits in $D = 1, 2$ both. Confirmation of this assumption should be a target of further research.

The autocorrelation and aging exponents which we found for the driven lattice gas of slopes differ from another two dimensional extension of the totally asymmetric exclusion process (TASEP) described in [63], where $\lambda_{C,s}/z = 1$ and $b_s = 1$ are reported.

Finally we point out that the SCA simulations are more efficient because they allow for optimal memory access patterns in contrast to the random accesses required for the RS ones. Technical details of our implementations are published elsewhere [38, 40]. The extension of these algorithms for other surface models, like those with conservation laws [64, 65] or in higher dimensions [33] is straightforward.

Acknowledgments:

We are grateful for the useful comments from Malte Henkel and Timothy Halpin-Healy and thank Herbert Spohn and Uwe Täuber for helpful discussions. Support from the Hungarian research fund OTKA (Grant No. K109577), the Initiative and Networking Fund of the Helmholtz Association via the W2/W3 Programm (W2/W3-026) and the International Helmholtz Research School NanoNet (VH-KO-606) is acknowledged. We gratefully acknowledge computational resources provided by the HZDR computing center, NIIF Hungary and the Center for Information Services and High Performance Computing (ZIH) at TU Dresden.

- [1] J. Marro and R. Dickman, *Nonequilibrium Phase Transitions in Lattice Models*, Collection Alea-Saclay: Monographs and Texts in Statistical Physics (Cambridge University Press, 2005), ISBN 9780521019460, URL <https://books.google.de/books?id=80YF69jbczYC>.
- [2] J. Krug, *Advances in Physics* **46**, 139 (1997), URL <http://dx.doi.org/10.1080/00018739700101498>.
- [3] T. Halpin-Healy and Y.-C. Zhang, *Physics Reports* **254**, 215 (1995), ISSN 0370-1573, URL <http://www.sciencedirect.com/science/article/pii/037015739400087J>.
- [4] U. C. Täuber, *Critical Dynamics* (Cambridge University Press, 2014), ISBN 9781139046213, Cambridge Books Online, URL <http://dx.doi.org/10.1017/CB09781139046213>.
- [5] G. Ódor, *Universality in Nonequilibrium Lattice Systems* (World Scientific, 2008).
- [6] F. Spitzer, *Advances in Mathematics* **5**, 246 (1970), ISSN 0001-8708, URL <http://www.sciencedirect.com/science/article/pii/0001870870900344>.
- [7] P. Meakin, P. Ramanlal, L. M. Sander, and R. C. Ball, *Phys. Rev. A* **34**, 5091 (1986), URL <http://link.aps.org/doi/10.1103/PhysRevA.34.5091>.
- [8] M. Plischke, Z. Rácz, and D. Liu, *Phys. Rev. B* **35**, 3485 (1987), URL <http://link.aps.org/doi/10.1103/PhysRevB.35.3485>.
- [9] M. Kardar, G. Parisi, and Y.-C. Zhang, *Phys. Rev. Lett.* **56**, 889 (1986), URL <http://link.aps.org/doi/10.1103/PhysRevLett.56.889>.
- [10] J. M. Burgers, *The nonlinear diffusion equation : asymptotic solutions and statistical problems* (Dordrecht-Holland ; Boston : D. Reidel Pub. Co, 1974), ISBN 9027704945, first published in 1973 under title: Statistical problems connected with asymptotic solutions of the one-dimensional nonlinear diffusion equation.
- [11] T. Halpin-Healy, *Phys. Rev. A* **42**, 711 (1990), URL <http://link.aps.org/doi/10.1103/PhysRevA.42.711>.
- [12] D. Forster, D. R. Nelson, and M. J. Stephen, *Phys. Rev. A* **16**, 732 (1977), URL <http://link.aps.org/doi/10.1103/PhysRevA.16.732>.
- [13] M. Kardar, *Phys. Rev. Lett.* **55**, 2923 (1985), URL <http://link.aps.org/doi/10.1103/PhysRevLett.55.2923>.
- [14] H. van Beijeren, R. Kutner, and H. Spohn, *Phys. Rev. Lett.* **54**, 2026 (1985), URL <http://link.aps.org/doi/10.1103/PhysRevLett.54.2026>.
- [15] H. Janssen and B. Schmittmann, *Zeitschrift für Physik B Condensed Matter* **63**, 517 (1986), ISSN 0722-3277, URL <http://dx.doi.org/10.1007/BF01726201>.
- [16] T. Hwa, *Phys. Rev. Lett.* **69**, 1552 (1992), URL <http://link.aps.org/doi/10.1103/PhysRevLett.69.1552>.
- [17] S. F. Edwards and D. R. Wilkinson, *Proc. R. Soc. London, Ser. A* **381**, 17 (1982), ISSN 0080-4630.
- [18] A. Barabási and H. Stanley, *Fractal Concepts in Surface Growth* (Cambridge University Press, 1995), ISBN 9780521483186, URL <https://books.google.de/books?id=W4SqCnr8PLYC>.
- [19] E. Marinari, A. Pagnani, G. Parisi, and Z. Rácz, *Phys. Rev. E* **65**, 026136 (2002), URL <http://link.aps.org/doi/10.1103/PhysRevE.65.026136>.
- [20] G. Foltin, K. Oerding, Z. Rácz, R. L. Workman, and R. K. P. Zia, *Phys. Rev. E* **50**, R639 (1994), URL <http://link.aps.org/doi/10.1103/PhysRevE.50.R639>.
- [21] M. Prähofer and H. Spohn, *Phys. Rev. Lett.* **84**, 4882 (2000), URL <http://link.aps.org/doi/10.1103/PhysRevLett.84.4882>.
- [22] T. Sasamoto and H. Spohn, *Phys. Rev. Lett.* **104**, 230602 (2010), URL <http://link.aps.org/doi/10.1103/PhysRevLett.104.230602>.
- [23] J.-L. Barrat, M. Feigelman, J. Kurcha, and J. Dalibard, *Slow Relaxations and Nonequilibrium Dynamics in Condensed Matter*, vol. 77 of *Les Houches - Ecole d'Ete de Physique Theorique* (Springer, 2003), ISBN 978-3-540-40141-4.
- [24] M. Krech, *Phys. Rev. E* **55**, 668 (1997), URL <http://link.aps.org/doi/10.1103/PhysRevE.55.668>.
- [25] M. Krech, *Phys. Rev. E* **56**, 1285 (1997), URL <http://link.aps.org/doi/10.1103/PhysRevE.56.1285>.
- [26] T. Kloss, L. Canet, and N. Wschebor, *Phys. Rev. E* **86**, 051124 (2012), URL <http://link.aps.org/doi/10.1103/PhysRevE.86.051124>.
- [27] H. Kallabis and J. Krug, *EPL* **45**, 20 (1999), URL <http://stacks.iop.org/0295-5075/45/i=1/a=020>.
- [28] M. Henkel and M. Pleimling, *Non-Equilibrium Phase Transitions: Volume 2: Ageing and Dynamical Scaling Far from Equilibrium*, Theoretical and Mathematical Physics (Springer Netherlands, 2010), ISBN 9789048128686, URL <https://books.google.de/books?id=DN2gjwEACAAJ>.
- [29] J. Kelling, G. Ódor, and S. Gemming (2016), to be published.
- [30] M. Henkel, *Nuclear Physics B* **869**, 282 (2013), ISSN 0550-3213, URL <http://www.sciencedirect.com/science/article/pii/S0550321312006682>.
- [31] J. Krug and H. Spohn, pp. 479–582 (1991).
- [32] G. Ódor, B. Liedke, and K.-H. Heinig, *Phys. Rev. E* **79**, 021125 (2009).
- [33] G. Ódor, B. Liedke, and K.-H. Heinig, *Phys. Rev. E* **81**, 031112 (2010), URL <http://link.aps.org/doi/10.1103/PhysRevE.81.031112>.
- [34] N. Rajewsky, L. Santen, A. Schadschneider, and M. Schreckenberg, *Journal of Statistical Physics* **92**, 151 (1998), ISSN 0022-4715, URL <http://dx.doi.org/10.1023/A%3A1023047703307>.
- [35] H. Schulz, G. Ódor, G. Ódor, and M. F. Nagy, *Comp. Phys. Comm.* **182**, 1467 (2011), URL <http://dblp.uni-trier.de/db/journals/cphysics/cphysics182.html#Schulz00N11>; <http://dx.doi.org/10.1016/j.cpc.2011.03.016>.
- [36] R. Juhász and G. Ódor, *Journal of Statistical Mechanics: Theory and Experiment* **2012**, P08004 (2012), URL <http://stacks.iop.org/1742-5468/2012/i=08/a=P08004>.
- [37] E. Marinari, A. Pagnani, and G. Parisi, *Journal of Physics A: Mathematical and General* **33**, 8181 (2000), URL <http://stacks.iop.org/0305-4470/33/i=46/a=303>.
- [38] J. Kelling, G. Ódor, and S. Gemming, in *2016 IEEE International Conference on Intelligent Engineering Systems, 2016. INES '16* (IEEE, 2016).
- [39] G. Ódor, J. Kelling, and S. Gemming, *Phys. Rev. E* **89**, 032146 (2014), URL <http://link.aps.org/doi/10.1103/PhysRevE.89.032146>.

- [40] J. Kelling, G. Ódor, and S. Gemming (2016), to be published.
- [41] K. Levenberg, Quarterly Journal of Applied Mathematics **II**, 164 (1944).
- [42] D. W. Marquardt, Journal of the Society for Industrial and Applied Mathematics **11**, 431 (1963), <http://dx.doi.org/10.1137/0111030>, URL <http://dx.doi.org/10.1137/0111030>.
- [43] T. Williams, C. Kelley, C. Bersch, H.-B. Bröker, J. Campbell, R. Cunningham, D. Denholm, G. Elber, R. Fearick, C. Grammes, et al., *Gnuplot: an interactive plotting program*, <http://www.gnuplot.info> (2015).
- [44] A. Röthlein, F. Baumann, and M. Pleimling, Phys. Rev. E **74**, 061604 (2006), URL <http://link.aps.org/doi/10.1103/PhysRevE.74.061604>.
- [45] A. Röthlein, F. Baumann, and M. Pleimling, Phys. Rev. E **76**, 019901 (2007), URL <http://link.aps.org/doi/10.1103/PhysRevE.76.019901>.
- [46] J. Kelling and G. Ódor, Phys. Rev. E **84**, 061150 (2011), URL <http://link.aps.org/doi/10.1103/PhysRevE.84.061150>.
- [47] T. Halpin-Healy, Phys. Rev. Lett. **109**, 170602 (2012), URL <http://link.aps.org/doi/10.1103/PhysRevLett.109.170602>.
- [48] T. J. Oliveira, S. G. Alves, and S. C. Ferreira, Phys. Rev. E **87**, 040102 (2013), URL <http://link.aps.org/doi/10.1103/PhysRevE.87.040102>.
- [49] T. Paiva and F. Aarão Reis, Surface Science **601**, 419 (2007), ISSN 0039-6028, URL <http://www.sciencedirect.com/science/article/pii/S0039602806010661>.
- [50] F. D. A. Aarão Reis, Phys. Rev. E **69**, 021610 (2004), URL <http://link.aps.org/doi/10.1103/PhysRevE.69.021610>.
- [51] P. L. Ferrari and R. Frings, Journal of Statistical Physics **144**, 1123 (2011), ISSN 1572-9613, URL <http://dx.doi.org/10.1007/s10955-011-0318-4>.
- [52] S. G. Alves, T. J. Oliveira, and S. C. Ferreira, Journal of Statistical Mechanics: Theory and Experiment **2013**, P05007 (2013), URL <http://stacks.iop.org/1742-5468/2013/i=05/a=P05007>.
- [53] T. Halpin-Healy and Y. Lin, Phys. Rev. E **89**, 010103 (2014), URL <http://link.aps.org/doi/10.1103/PhysRevE.89.010103>.
- [54] E. A. Rodrigues, B. A. Mello, and F. A. Oliveira, Journal of Physics A: Mathematical and Theoretical **48**, 035001 (2015), URL <http://stacks.iop.org/1751-8121/48/i=3/a=035001>.
- [55] T. Halpin-Healy and G. Palasantzas, EPL **105**, 50001 (2014), URL <http://stacks.iop.org/0295-5075/105/i=5/a=50001>.
- [56] A. Pagnani and G. Parisi, Phys. Rev. E **92**, 010101 (2015), URL <http://link.aps.org/doi/10.1103/PhysRevE.92.010101>.
- [57] J. Kelling, G. Ódor, and S. Gemming, Phys. Rev. E **94**, 022107 (2016), URL <http://link.aps.org/doi/10.1103/PhysRevE.94.022107>.
- [58] T. Halpin-Healy, Phys. Rev. E **88**, 042118 (2013), URL <http://link.aps.org/doi/10.1103/PhysRevE.88.042118>.
- [59] B. M. Forrest and L.-H. Tang, Phys. Rev. Lett. **64**, 1405 (1990), URL <http://link.aps.org/doi/10.1103/PhysRevLett.64.1405>.
- [60] H. S. Wio, J. A. Revelli, R. R. Deza, C. Escudero, and M. S. de la Lama, EPL (Europhysics Letters) **89**, 40008 (2010), URL <http://stacks.iop.org/0295-5075/89/i=4/a=40008>.
- [61] U. Dekker and F. Haake, Phys. Rev. A **11**, 2043 (1975), URL <http://link.aps.org/doi/10.1103/PhysRevA.11.2043>.
- [62] M. Henkel, J. D. Noh, and M. Pleimling, Phys. Rev. E **85**, 030102 (2012), URL <http://link.aps.org/doi/10.1103/PhysRevE.85.030102>.
- [63] G. L. Daquila and U. C. Täuber, Phys. Rev. E **83**, 051107 (2011), URL <http://link.aps.org/doi/10.1103/PhysRevE.83.051107>.
- [64] G. Ódor, B. Liedke, and K.-H. Heinig, Phys. Rev. E **81**, 051114 (2010), URL <http://link.aps.org/doi/10.1103/PhysRevE.81.051114>.
- [65] G. Ódor, B. Liedke, H. Karl-Heinz, and J. Kelling, Applied Surface Science **258** (2012).
- [66] The cut-off was observed at $\tilde{t}' \approx 1.7 \times 10^5$ MCS at two different times contributing in the calculation of $\beta_{\text{eff}}(\tilde{t}')$: $\tilde{t}_1 \approx 2 \times 10^4$ MCS and $\tilde{t}_2 \approx 3.2 \times 10^5$ MCS $\gtrsim t_{\text{fs}}$.
- [67] These limits could also be determined from the small survey study presented in Figure 2(a), comprising much smaller sample sizes than the results presented in detail in the following. This data suggests an exponential dependence $o(p) \propto \exp(\nu p)$ with a similar, or possibly the same, value for the parameter ν for both slopes and heights. However, these autocorrelation measurements used the same waiting time s , without taking into account the p -dependent time-scale. Thus the actual waiting times \tilde{s} decrease with p , which makes the fit performed on the $o(p)$ across these runs unsuitable to determine a reliable value for ν .